Integrated multidimensional positioner for precision manufacturing

W-J Kim*, **N Bhat** and **T Hu**
Department of Mechanical Engineering, Texas A&M University, College Station, Texas, USA

Abstract: Reliable low-cost positioning for precision manufacturing processes requiring clean-room, extreme-temperature or vacuum environments is key for microelectronics manufacturing, packaging, machine tool and high-precision inspection industries. The integrated multidimensional positioner presented herein is a major technological breakthrough and may offer competitive advantages in both cost and performance relative to current practices. Specifically, this integrated positioner can generate all required fine and coarse motions with only one levitated moving part, namely the platen, and have potential to satisfy the dynamic performance specifications necessary for next-generation deep-submicron microelectronics manufacturing equipment. Absence of particulate contamination without mechanical contact between the single moving part and the machine frame makes this technology highly suited to clean-room operation. In this paper, the design concept, electromechanical design and fabrication and assembly of all the key parts in the development of this multidimensional positioner are presented. A dynamic model and feedback controllers were derived and implemented. This prototype positioner currently has a planar travelling range of 160 mm × 160 mm with a position resolution of 30 nm, position repeatability of 30 nm, position noise of 10 nm r.m.s. and platen dimensional stability of 32.7 μm. The maximum velocity achieved so far is 0.4 m/s with 2 m/s^2 acceleration. Various experimental results verified the utility of this positioner in precision manufacturing applications.

Keywords: precision manufacturing, clean manufacturing, multidimensional nanoscale positioning, microelectronics manufacturing, real-time digital control

NOTATION

f	modal force component (N)
G	geometric constant (m^3)
i_{kd}	direct current component (A)
i_{kq}	quadrature current component (A)
I_{xx}	moment of inertia about the x axis (kg m^2)
I_{yy}	moment of inertia about the y axis (kg m^2)
I_{zz}	moment of inertia about the z axis (kg m^2)
k	motors I, II or III
l	motor pitch (m)
N_m	number of active magnet pitches
P	power consumption by the motor (W)
w	magnet array width (m)
x	translation in the x direction (m)
y	translation in the y direction (m)
z	translation in the z direction (m)
z_0	nominal motor air gap (m)
α	linear coefficient of thermal expansion (m/m °C)
γ_1	absolute value of fundamental wave number (m$^{\times 1}$)
Λ	winding thickness (m)
ΔL_{max}	deformation of one side of the platen (m)
ΔT	change in the temperature (°C)
Δ	magnet array thickness (m)
η_0	winding turn density (m$^{\times 2}$)
θ	rotation about the x axis (rad)
$\mu_0 M_0$	magnet remanence (T)
ϕ	rotation about the z axis (rad)
ψ	rotation about the y axis (rad)

The MS was received on 17 June 2003 and was accepted after revision for publication on 7 January 2004.
**Corresponding author: Department of Mechanical Engineering, Texas A&M University, College Station, TX 77843-3123, USA.*

1 INTRODUCTION

Besides shrinking feature size and demanding overlay accuracy, transitioning the wafer size to 300 mm in diameter and beyond will introduce significant design challenges in microelectronics manufacturing and material handling automation. For example, an unprocessed 300 mm wafer is more than twice as heavy as a

200 mm wafer (125 g versus 56 g). Thus, the mass of 25 300 mm wafers together with their film frame and cassette will be over 13.5 kg, which will double the mass of the cassette of 25 200 mm wafers currently being used [**1**]. It will introduce significant changes in wafer dicing, mounting, die-attach machines, pod door openers, stockers and handling robots, increasing footprints, and force and power requirements. However, the conventional wafer-handling technologies for 200 mm wafers may not be able to meet the new specifications and many technical challenges of this transition to 300 mm wafers. Therefore, reliable low-cost positioning for precision manufacturing processes requiring clean room, extreme-temperature or vacuum environments is key for microelectronics manufacturing, packaging, machine tool and high-precision inspection industries.

The integrated multidimensional motion generation technology presented in this paper is a major technological breakthrough and offers competitive advantages in both cost and performance relative to current practices. Specifically, this multidimensional positioner can generate all required fine and coarse motions with only one levitated moving part and has potential to satisfy the dynamic performance specifications necessary for next-generation deep-submicron microelectronics manufacturing equipment. For example, this single-moving-part positioner can be used as a wafer stepper in photolithography in microelectronics manufacturing by generating step-and-still and scanning motions in the x and y axes independently. Focusing and local levelling of the silicon wafer can also be performed without employing additional actuators. Absence of particulate contamination without mechanical contact between the single moving part and the machine frame makes this technology highly suited to clean-room operations. It may also replace conventional track systems and robot arms in cluster chambers in a more reliable and cost-effective way.

Many researchers have studied the control of planar motions. An early example is the Sawyer motor that is a variable-reluctance type and has frequently been used without explicit position feedback [**2**]. The reported step resolution is on the order of 250 μm. Since its primary application was x–y plotters, this relatively low resolution was sufficient. For precision motion control with a particular emphasis on wafer stepper stages, Hinds and Nocito [**3**] and Pelta [**4**] improved the original version of the Sawyer motor. There are several companies that commercialized this Sawyer motor such as Ultratech, Northern Magnetics and Megamation. However, this Sawyer-motor technology has significant drawbacks for use in precision positioning applications.

1. The Sawyer motor needs tight air gap less than 25 μm, and so it requires an ultrafine surface finish of the motor surfaces.
2. Its position repeatability is only as good as 5 μm.
3. In addition to a large cogging force, the attractive force of one commercial system is as large as 1800 N [**5**].

Keeping pace with advances in permanent-magnet materials in the last decades, planar positioning concepts using permanent magnet were presented by Asakawa [**6**] and Ebihara and Watada [**7**]. Some of these systems utilize planar motors (or surface motors in some literature [**8**]). Another planar motion system, which led to the SVGL Micrascan system, was designed by Buckley *et al*. [**9**]. It has two unipolar permanent-magnet planar motors to generate major two-dimensional motions and rotation about the normal to the stage. This wafer stage is constrained by aerostatic-bearing pads. The stages mentioned so far cannot provide focus range or local levelling without using fine-motion actuators.

The integrated multidimensional motion generator proposed herein overcame all the shortcomings of the established Sawyer motor technology. The prototype positioner achieved a 30 nm positioning resolution and 160 mm × 160 mm planar travel range without requiring additional primary coarse-motion or secondary fine-motion stages. The extension of the travel range can be achieved by adding more magnet pieces to the magnet matrix shown in Fig. 3 later, and is unlimited. This integrated multidimensional positioning approach has significant advantages:

1. A non-contact stage requires no lubricants, does not generate wear particles, is non-contaminating and thus is highly suited to clean-room environments.
2. The footprint is reduced by superimposing multiple linear motors into one unified actuation system.
3. The single moving part can be designed to have high natural frequencies compared with prevailing multi-element stages with complex dynamics.
4. By eliminating complicated mechanical elements, the fabrication cost is reduced and the reliability is increased.
5. It does not require excessive surface finish.
6. Its cogging force will be less than a fraction of a newton without a strong attractive force [**10**].

Therefore, this integrated multi-axis motion generation technology holds promise for future precision manufacturing and automation applications.

The design concept and working principle of the positioner are presented in section 2. In section 3 the design and fabrication of the base plate including the novel concentrated-field magnet matrix are discussed in detail. Section 4 presents the design and assembly of the moving platen. Section 5 describes the dynamics and control of the positioning system focusing on the electromechanical design, force allocation and controller design. The instrumentation structure for this positioner is also discussed in this section. The test results presented in section 6 demonstrate its performance characteristics and precise multidimensional positioning capability.

2 INTEGRATED MULTIDIMENSIONAL POSITIONER

2.1 Design concept

Figure 1 shows a photograph of the integrated multidimensional positioner and a perspective view of the whole hardware set-up. The triangular single-moving part, namely the platen, carries the winding sets that energize the actuation system. Each winding set on the bottom surface of the platen interacts with the magnet matrix and generates independent vertical and horizontal force components that follow the Lorentz force law [11]. In other words, the coil currents in the x and y windings generate an air-gap magnetic field travelling in the x and y directions respectively. Consequently, each of the x- and y-winding currents interacts only with the corresponding x- and y-magnet matrix component to be described in section 3. This concept provides means to stabilize and control actively all the six-axis translational and rotational motions.

2.2 Working principle

The platen carries the three linear-motor winding sets I, II and III, as shown in Fig. 2a. Motors I and II generate

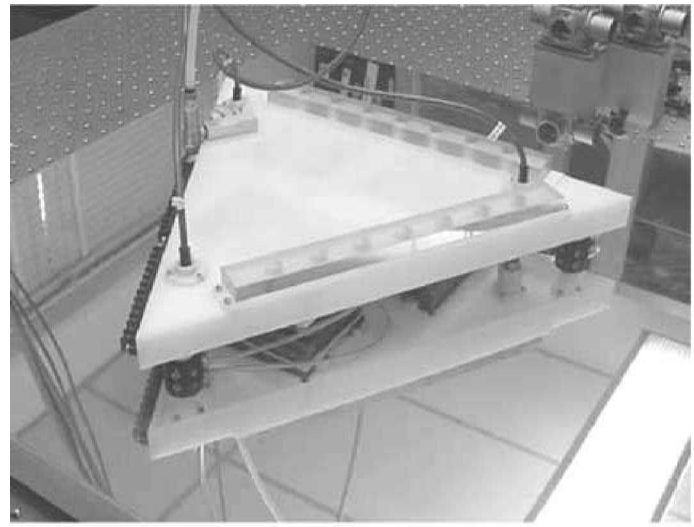

(a)

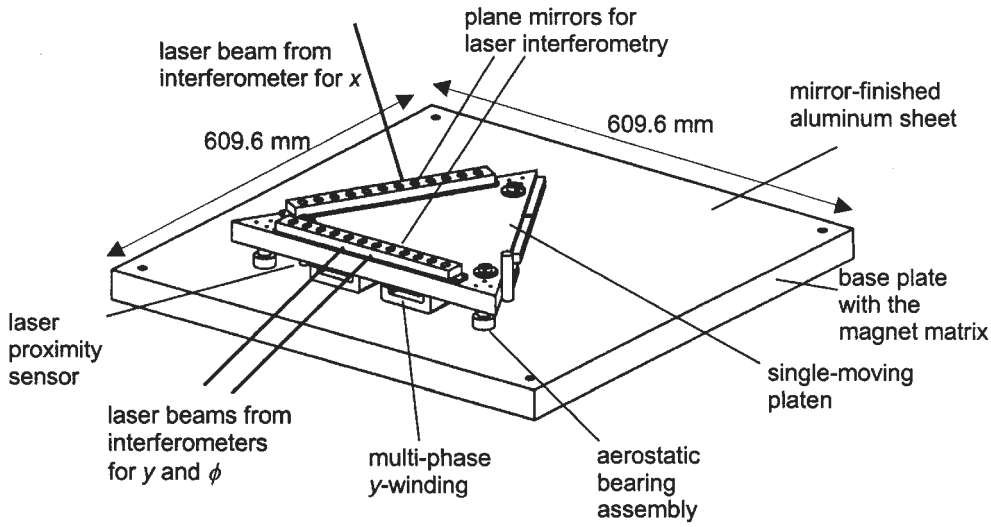

(b)

Fig. 1 (a) Photograph of the integrated multidimensional positioner. (b) Perspective view. The base plate is covered by a mirror-finished aluminium sheet, and hence in the photograph the reflection of parts such as overhead lights is seen. The magnet matrix is present beneath this mirror-finished aluminium sheet in the base plate

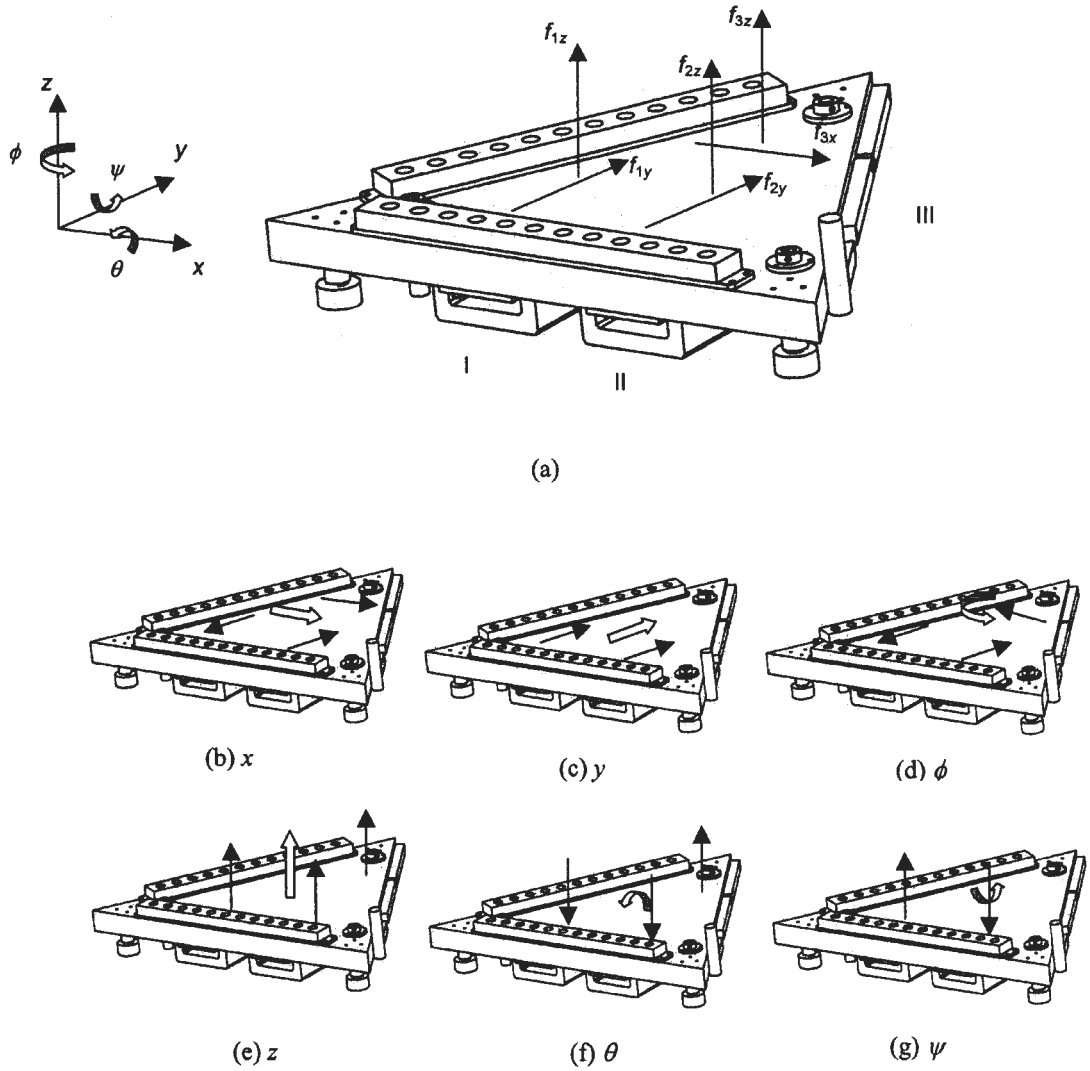

Fig. 2 (a) Convention of the coordinate axes and the directions of forces by each linear motor. The origin of the coordinate system coincides with the platen centre of mass. Roman numerals I, II and III denote the winding sets of the three linear motors respectively. For exact location of the winding set III, refer to Fig. 5b. (b)–(g) The force allocations to generate all the six-axis motions. The thin arrows indicate the modal force components produced by individual linear motors. The thick white arrows represent the resultant modal force/torque acting on the platen centre of mass

y-directional forces, and motor III generates an x-directional force. Each of the three motors can also generate the z-directional forces independently, as will be explained in section 5.1. The conceptual modal force generation of the integrated multidimensional positioning system is depicted in Fig. 2a. Figures 2b–g show the directions of forces by individual linear motors to generate the platen motion in any particular axis. For example, positive f_{3x} produces a translational motion in the positive x direction as shown in Fig. 2b. In this particular case, f_{3x} does not act on the platen centre of mass; therefore positive f_{2y} and negative f_{1y} must be generated to cancel the torque component about the z axis. A positive rotational motion about the z axis is obtained with positive f_{2y}, negative f_{1y} and negative f_{3x}, as depicted in Fig. 2d. Motions in the four other degrees of freedom (DOFs) can be generated likewise. Hence this integrated positioner can generate all the forces required to move the single-moving platen in all six DOFs.

3 DESIGN AND FABRICATION OF THE BASE PLATE

3.1 Concentrated-field magnet matrix

Figure 3 shows the novel concentrated-field magnet matrix that produces the constant magnetic field for actuation [**12**]. This magnet matrix can be produced conceptually by the superimposition of two orthogonal Halbach arrays [**13**], as shown in Fig. 3a. In Fig. 3b, magnet blocks with an arrow have $1/\sqrt{2}$ remanence of

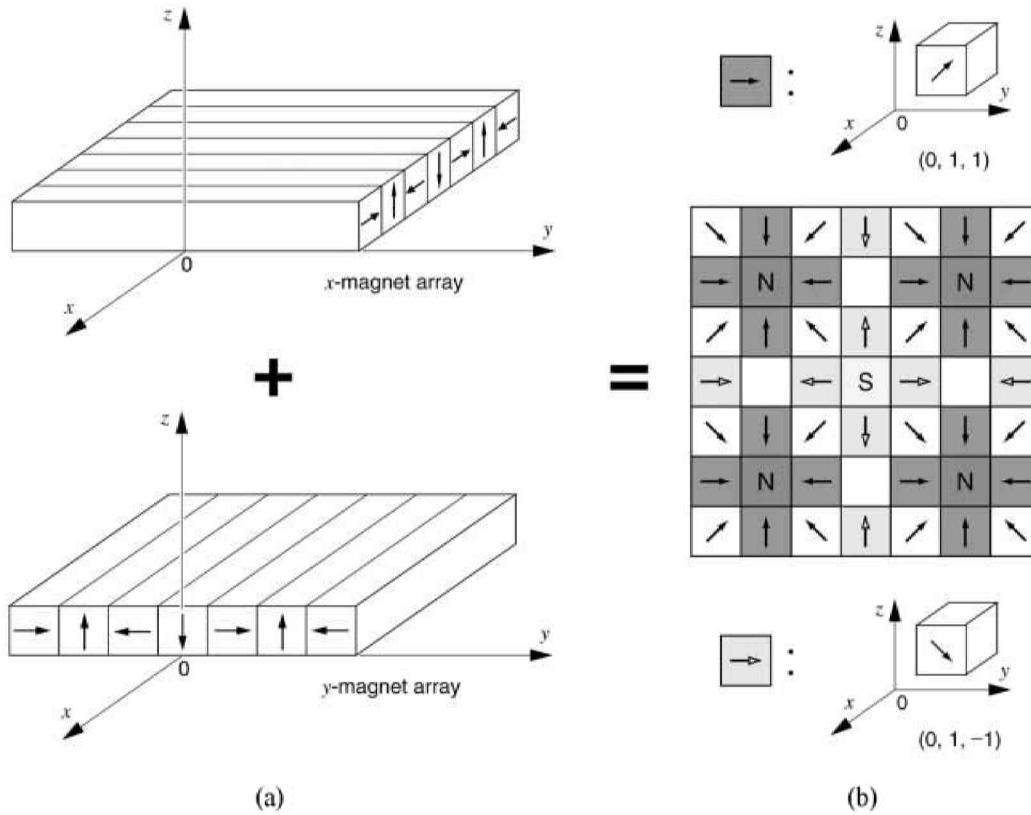

Fig. 3 (a) Conceptual superimposition of the two orthogonal Halbach magnet arrays to produce a concentrated-field magnet matrix. (b) Top view of the concentrated-field magnet matrix. In the current prototype positioner, there are 24 × 24 individual magnet pieces in the matrix

the magnets denoted with north (N) and south (S) poles. Shaded blocks with solid arrows tip up at 45° whereas shaded blocks with hollow arrows tip down at 45°. The Halbach array has a stronger fundamental field by the factor of $\sqrt{2}$. This will also be the case with the two-dimensional magnet matrices, since the magnetic fields obey linear superposition. By using such an array we can achieve higher power efficiency than those which utilize conventional magnetization patterns [**11**]. As mentioned earlier, the magnet matrix in the positioner is present in the stationary base plate. The number of pitches on the magnet matrix determines the travel range of the positioner. In our prototype design the whole magnet matrix has six pitches in the x and y directions respectively, giving a 160 mm × 160 mm planar travel range.

3.2 Fabrication of the magnet matrix

The magnet matrix in our positioner contains 72 magnets with the conventional magnetization direction and 432 magnets with the diagonal magnetization direction, and 72 non-magnetic aluminium spacers. The dimension of all the magnet pieces and the aluminium spacers is 12.7 mm × 12.7 mm × 12.7 mm with a dimensional tolerance of ±50 μm. For the magnets with the conventional magnetization direction, NdFeB50 material with a remanence of 1.43 T was chosen. The other magnets with the diagonal magnetization direction were NdFeB30 with a remanence of 1.10 T. All the magnets have phenolic resin coating to prevent corrosion.

To glue the magnets together, PC-7 epoxy was chosen as it adhered very well to the phenolic resin coating. The magnet matrix was assembled in a pocket of 307.97 mm × 307.97 mm × 13.716 mm milled in an aluminium base plate of 609.6 mm × 609.6 mm × 38.1 mm. The glue-line thickness between the magnets was maintained at 0.254 mm. In the pocket, 576 clearance holes with 6.35 mm diameter and of depth 12.7 mm were made at a distance of 12.7 mm from each other such that each hole faced exactly the centre of each magnet. They were made to give leverage to the tool, which was designed to push the magnets next to each other in the assembly process. The tool used to push the magnets consisted of a channel of 64.62 mm × 12.954 mm × 13.03 mm with a plunger behind it. After the completion of one row, all the set screws in the holder were re-examined to ascertain that equal forces were applied to each magnet. In this manner all the 24 rows were assembled at a rate of four rows a day with a curing time of 24 h. Figure 4 shows the magnet matrix after glueing 12 such rows.

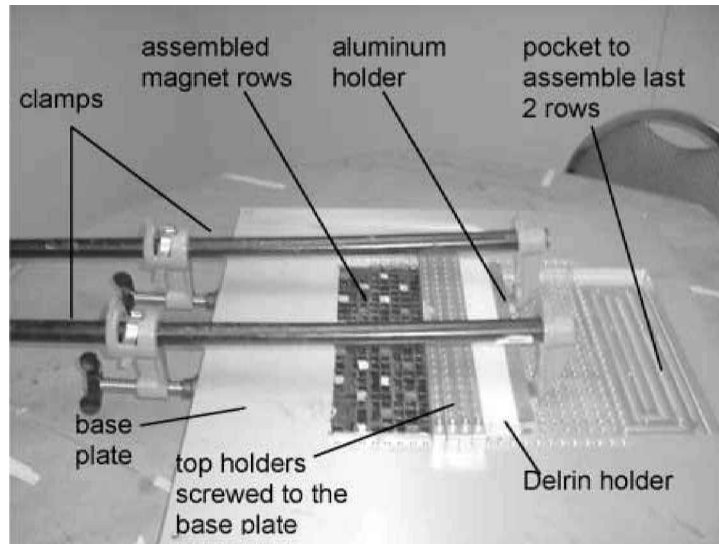

Fig. 4 Photograph showing the magnet matrix in the stage of assembly where eight rows were completed previously. It shows the completion of another set of four rows being held by the four top holders and the clamp assembly

3.3 Base plate assembly

Aerostatic bearings, which are critical to provide the suspension force for the platen, require a target with a fine surface finish of $\pm 20\,\mu m$. To achieve this surface finish over the magnet matrix would be a significant challenge. Initially a layer of epoxy approximately 1.27 mm thick was spread over the whole magnet matrix surface. After the epoxy was cured, the base plate was mounted over a large chuck of a lathe. The surface was milled and epoxy approximately 0.762 mm thick was removed. The resultant thickness of the epoxy layer over the magnet matrix was calculated to be 0.508 mm by a coordinate measuring machine. The entire surface had good 25.4 μm flatness with numerous small pores due to uneven mixing of epoxy. Thus, to provide with a good finished surface for the optimum performance of the aerostatic bearings, a mirror-finished aluminium sheet of dimensions 609.6 mm × 609.6 mm × 1.016 mm was placed over the entire base plate. The manufacturer guarantees the surface flatness of 0.1 μm for this aluminium sheet.

4 DESIGN AND FABRICATION OF THE MOVING PLATEN

4.1 Winding set

To form one linear motor winding set, 12 Gramme windings were stacked side by side [**11**]. Various winding parameters such as thickness of wire, number of layers, number of turns, together with the peak phase current and terminal voltage required many design iterations. The dimensions of the coil are 45.78 mm × 72.59 mm × 8.496 mm. One motor has 12 coils; therefore the overall dimension of one linear-motor winding set is 45.78 mm × 72.59 mm × 101.95 mm. The pitch of the motor is 50.977 mm. According to the specifications the American Wire Gauge 24 wire has a resistivity of $0.08422\,\Omega/m$. The resistance of one winding was measured to be $4.86\,\Omega$. The cross-sectional area of one winding is $8.6534 \times 10^{\times 5}\,m^2$.

4.2 Platen assembly

Figure 5 shows exploded views of the platen from the top and bottom. The platen was designed in an equilateral triangular shape for compactness with 381 mm length and 25.4 mm thickness. White Delrin (a trade name of Acetal) was chosen to be the material for the platen because of its low mass density of $1.43\,g/cm^3$. Three linear motor winding sets, three laser distance sensors, two plane mirrors for the interferometers, three aerostatic bearings and their air distributor, and terminal blocks are mounted on this platen. Three ceramic aerostatic bearings manufactured by Nelson Air Corporation were mounted at the three corners of the triangular platen (Fig. 5b), to provide vertical suspension. The nominal gap between the air bearings and the mirror-finished aluminium sheet is 25 μm.

On the bottom side of the platen, three 75.15 mm × 105 mm × 19.05 mm pockets with a dimensional tolerance of ±0.127 mm were made for the three linear-motor winding sets. To decrease the total mass of the system additional four pockets were made on the platen, as shown in Fig. 5b. A finite element analysis showed that the first resonant mode of the platen was as high as 1689.1 Hz. Although it was possible to levitate

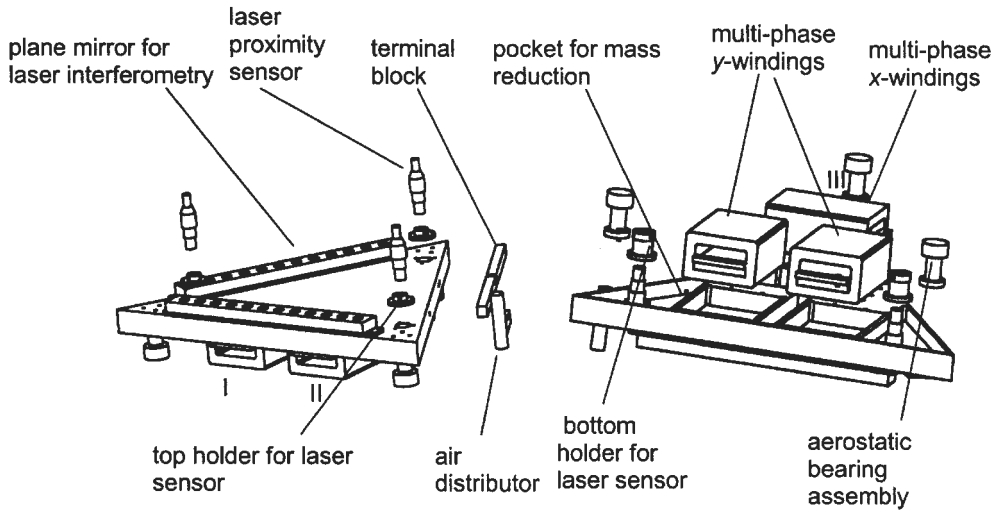

Fig. 5 Exploded view of the platen assembly from (a) the top and (b) the bottom

the positioner electromagnetically, aerostatic bearings were used to suspend the platen against gravity to reduce power consumption significantly.

5 DYNAMIC MODELLING AND CONTROL

5.1 Force equations

For modelling purposes, the mechanical parameters of the platen were derived. The mass M of the platen was measured as 5.91 kg by a precision balance. The moments of inertia about the coordinate axes depicted in Fig. 2 were calculated as $I_{xx} = 0.033\,\mathrm{kg\,m^2}$, $I_{yy} = 0.025\,\mathrm{kg\,m^2}$ and $I_{zz} = 0.054\,\mathrm{kg\,m^2}$ with SolidWorks. The products of inertia, I_{xy}, I_{yz} and I_{zx}, were negligible.

The vertical and lateral force components in the quadrature and direct current components i_{kq} and i_{kd} were derived as [**11**, **14**]

$$f_{k(x,y)} = \tfrac{1}{2}\mu_0 M_0 \eta_0 N_m G\, e^{\times\gamma_1 z_0} i_{kq}$$
$$f_{kz} = \tfrac{1}{2}\mu_0 M_0 \eta_0 N_m G\, e^{\times\gamma_1 z_0} i_{kd} \tag{1}$$

where the index k represents motors I, II or III and G is a geometric constant given as $G = (\sqrt{2} w l^2/\pi^2)\times(1 \times e^{\times\gamma_1 \Lambda})(1 \times e^{\times\gamma_1 \Delta})$. For our design, the parameters have the following values: the magnet remanence is $\mu_0 M_0 = 0.715\,\mathrm{T}$; the winding turn density is $\eta_0 = 3.5246 \times 10^6\,\mathrm{turns/m^2}$; the number of active magnet pitches is $N_m = 2$; the pitch is $l = 50.977\,\mathrm{mm}$; the absolute value of fundamental wave number is $\gamma_1 = |2\pi/l| = 123.25\,\mathrm{m}^{\times 1}$; the magnet array width $w = 50.977\,\mathrm{mm}$; the magnet array thickness $\Delta = 12.7\,\mathrm{mm}$; the winding thickness $\Lambda = 10.16\,\mathrm{mm}$; the nominal motor air gap $z_0 = 2.324\,\mathrm{mm}$. The constant G was then calculated to be $1.0722 \times 10^{\times 5}\,\mathrm{m^3}$ with these parameters. Substituting the above parameter values specific to the present motors,

$$\begin{bmatrix} f_{k(x,y)} \\ f_{kz} \end{bmatrix} = 20.15\,\mathrm{N/A} \begin{bmatrix} i_{kq} \\ i_{kd} \end{bmatrix} \tag{2}$$

yields the motor horizontal and vertical forces proportional to the corresponding current components.

For the control of translational motions in the x and y directions, the platen is modelled as a pure mass. Because there is no friction between the base plate and the platen levitated by aerostatic bearings, the dynamics of this pure mass model was presented by the Newton equation of motion

$$M \frac{d^2 x}{dt^2} = f \tag{3}$$

where M is equal to 5.91 kg and f is the magnetic modal force generated by the motors. Then the open-loop transfer function for translation motion becomes

$$\frac{X(s)}{F(s)} = \frac{1}{5.91 s^2} \tag{4}$$

5.2 Thermal drift and dimensional stability

As a wafer stage in photolithography in semiconductor manufacturing, the platen would be operated to generate swift coarse back-and-forth motions repeatedly. At the same time, it would generate precise fine motions to align and focus the silicon wafer. In both the cases, the positioner consumes electric power that leads to heat generation whenever it accelerates and decelerates. These coarse- and fine-motion operating conditions of

the positioner are analysed in this section to estimate thermal drift and dimensional stability.

The maximum acceleration of the platen is $2\,\mathrm{m/s^2}$ in the y direction, which corresponds to a force generation of 11.82 N (recall that the mass of the platen is 5.91 kg). From the force equation (2), representative nominal phase currents of one motor could be $i_A = 0.2933\,\mathrm{A}$, $i_B = 0.1467\,\mathrm{A}$ and $i_C = \times 0.1467\,\mathrm{A}$. As the resistance of a whole phase coil is $19.44\,\Omega$, the power consumption of one motor to generate $2\,\mathrm{m/s^2}$ acceleration is calculated to be approximately $P = (i_A^2 + i_B^2 + i_C^2)R = 2.5\,\mathrm{W}$. If the platen is operated with acceleration and deceleration periods of 0.2 s each to reach its maximum velocity, and if the overall period of the repetitive step-and-still motions is 1 s, the average power consumption by the two y motors can be computed as $P_{avg} = 2 \times 2 \times P \times 0.2\,\mathrm{s}/1\,\mathrm{s} = 2.0\,\mathrm{W}$. A heat transfer analysis indicates that this power consumption would raise the temperature of the platen by 1.06 °C on average at steady state. Suppose that the platen is heated uniformly by the motors; then the maximum thermal deformation of one side of the platen $\Delta L_{max} = \alpha L_{max} \Delta T = 81 \times 10^{\times 6}\,\mathrm{m/m\,°C} \times 0.381\,\mathrm{m} \times 1.06\,°\mathrm{C} = 32.7\,\mu\mathrm{m}$, where $\alpha = 81 \times 10^{\times 6}\,\mathrm{m/m\,°C}$ is Delrin's linear coefficient of thermal expansion [**15**], and $L_{max} = 0.381\,\mathrm{m}$ is the length of a side of the triangular platen.

The same methodology can be applied for the fine-motion operating condition. The instant phase currents of the motors were experimentally recorded with a digital signal processor (DSP). With these values, the average power consumption $P_{avg} = 12.6\,\mathrm{mW}$ was calculated in the motors, which would raise the temperature of the platen by $6.68 \times 10^{\times 3}$ °C. The corresponding maximum thermal deformation of one side of the platen is $\Delta L_{max} = 0.2\,\mu\mathrm{m}$.

From the calculation of thermal expansion under the two operating conditions, it can be seen that the dimensional stability of the platen is about 32.7 μm. Compared with the characteristic dimension of the whole platen of 0.381 m, this thermal error is negligible. Moreover, the feedback control compensates for this moderate thermal error.

5.3 Dynamic model and real-time digital control

The following digital lead-lag compensator for the translational motion control was designed and implemented at a sampling rate of 5 kHz with the model developed in section 5.1:

$$G_x(z) = 7.4 \times 10^5 \frac{z \times 0.9903}{z \times 0.7970} \frac{z \times 0.9979}{z \times 1} \tag{5}$$

The phase margin of the control system is 57.7° with a crossover frequency at 21 Hz.

For the control of rotation around the z axis, the dynamics of the system are represented by the differential equation

$$I_{zz} \frac{\mathrm{d}^2\phi}{\mathrm{d}t^2} = \tau \tag{6}$$

where τ is the torque from the magnetic origin around the z axis, and I_{zz} is the moment of inertia about the z axis. As $I_{zz} = 0.054\,\mathrm{kg\,m^2}$, the open-loop transfer function for the rotation around the z axis is

$$\frac{\Phi(s)}{T(s)} = \frac{1}{0.054s^2} \tag{7}$$

The implemented digital lead-lag compensator is

$$G_\phi(z) = 13062.95 \frac{z \times 0.9903}{z \times 0.7970} \frac{z \times 0.9979}{z \times 1} \tag{8}$$

with the phase margin of 62.7° with a crossover frequency at 38 Hz. Similarly, four additional lead-lag controllers were designed and implemented to control the motion in the four remaining axes.

5.4 Instrumentation structure

Figure 6 shows a schematic diagram of the instrumentation structure of the multidimensional positioning system. The Pentek 4284 board with a TMS320C40 DSP is employed for the real-time digital control of the system. Sampling of position data, control variable calculation and real-time control take place in an interrupt service routine. A VersaModule Eurocard (VME) personal computer (PC) (VMIC 7751) and three laser-axis boards (Agilent 10897B) are on the VME chassis along with the DSP board. The VME PC is used to compile the C codes, to download the executable file to the DSP and to transfer the commands in real time via the user interface during the system operation. This communication between the DSP and the VME PC is established via a dual-port memory on the DSP board.

The laser interferometer system consists of a laser head, three laser interferometers, beam benders, beam splitters, receivers, plane mirrors and laser-axis boards. An Agilent 5517D laser head is the 632 nm He–Ne laser source with the 1 m/s maximum slew rate. The three interferometers can give the three-DOF position information of the platen at a resolution of 0.6 nm. Digital 35 bit position and 24 bit velocity data are available directly from the laser-axis boards with a refresh rate of 10 MHz. Three laser distance sensors (Nanogage 100) are used for position feedback in the vertical axes. Their measuring range is 100 μm and resolution is 15 nm. These sensors pass the three vertical-axis position measurements to a data acquisition board through first-order RC anti-aliasing filters with a cut-off frequency of 1 kHz. The data-acquisition system contains eight channels of 16 bit analogue-to-digital converters (ADCs) (Pentek 6102) and 16 channels of 12 bit digital-to-analogue converters (DACs) (Datel

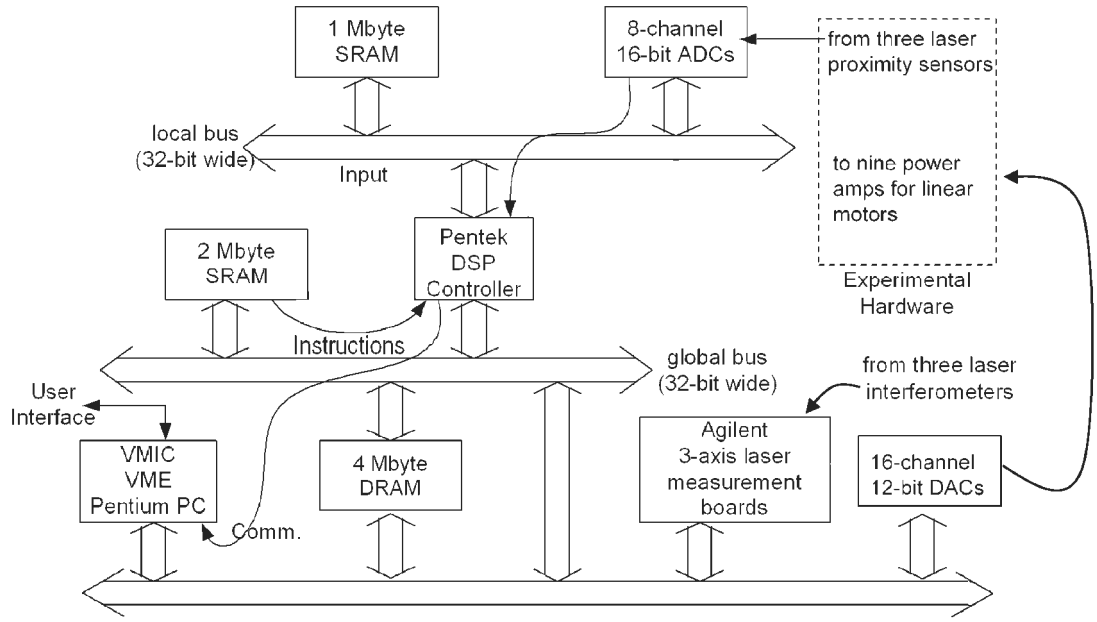

Fig. 6 Schematic diagram of the instrumentation structure (SRAM, semirandom access memory; DRAM, dynamic random access memory)

DVME-622) with an input–output voltage swing of ± 5 V. The ADC board communicates with the DSP via the MIXbus while the DAC board communicates via the VME bus. Nine DAC channels are used to give the control outputs to nine transconductance amplifiers. Then, these amplifiers flow commanded currents through the linear motor winding sets to generate the actuation forces.

6 EXPERIMENTAL RESULTS

In order to demonstrate the applicability of this integrated multidimensional positioner in precision manufacturing, numerous experiments were performed. Many manufacturing applications, such as microelectronics manufacturing, require a motion-generation stage to move the object from a position to another desired position as fast as possible. The step response of this integrated positioner with important transient characteristics such as rise time, settling time, percentage overshoot and steady state error is an effective indicator of its dynamic performance.

Figures 7a and b show closed-loop 10 μm step responses in the x and y directions respectively. The rise time is less than 10 ms, and the settling time is about 200 ms without steady state error. The percentage overshoots are about 60 per cent and 40 per cent in the x and y directions respectively. The more oscillatory behaviour in the x direction is believed to originate from the fact that motor III generates a perturbation torque. Although motors I and II would compensate for this torque, it might not have been completely cancelled due to some errors in the model. Figure 7c shows a 10 μrad step response in ϕ. The low-frequency (at about 10 Hz) disturbance is believed to be generated by the umbilical signal and power cables and air pipes connected to the platen. These step responses demonstrated the positioner's quick and precise positioning capability.

Figure 8a presents a 50 nm step response in x, which shows a position resolution better than 30 nm. There exists a 60 nm peak-to-peak (10 nm r.m.s.) position noise. The experimentally obtained frequency response plot given in Fig. 8b shows a dominant noise component centred at 85 Hz. The acoustic noise generated by the three aerostatic bearings is believed to contribute to the position noise and disturbance significantly.

Figure 9 shows a 500 nm staircase response in the y direction. As there are no hysteresis, friction, stiction and backlash in this positioning system, the repeatability of the positioner is as good as 30 nm, which is suitable for the submicron manufacturing industry. There are many factors that can affect the absolute accuracy of the positioner, such as dimensional stability, variation in ambient temperature, change in air density (wind), and drift in position sensors. The focus in this research was on the experimental demonstration of the fundamental working principles and the electromechanical design principles. In the microelectronics industry, a relative measure of accuracy is used in the form of an overlay accuracy among many layers in circuit printing. It is believed that the overlay accuracy of this current prototype multidimensional positioner can be as good as of the order of 100 nm considering the noise performance of the sensors and the ambient operation condition in the present authors' laboratory. However, the correction

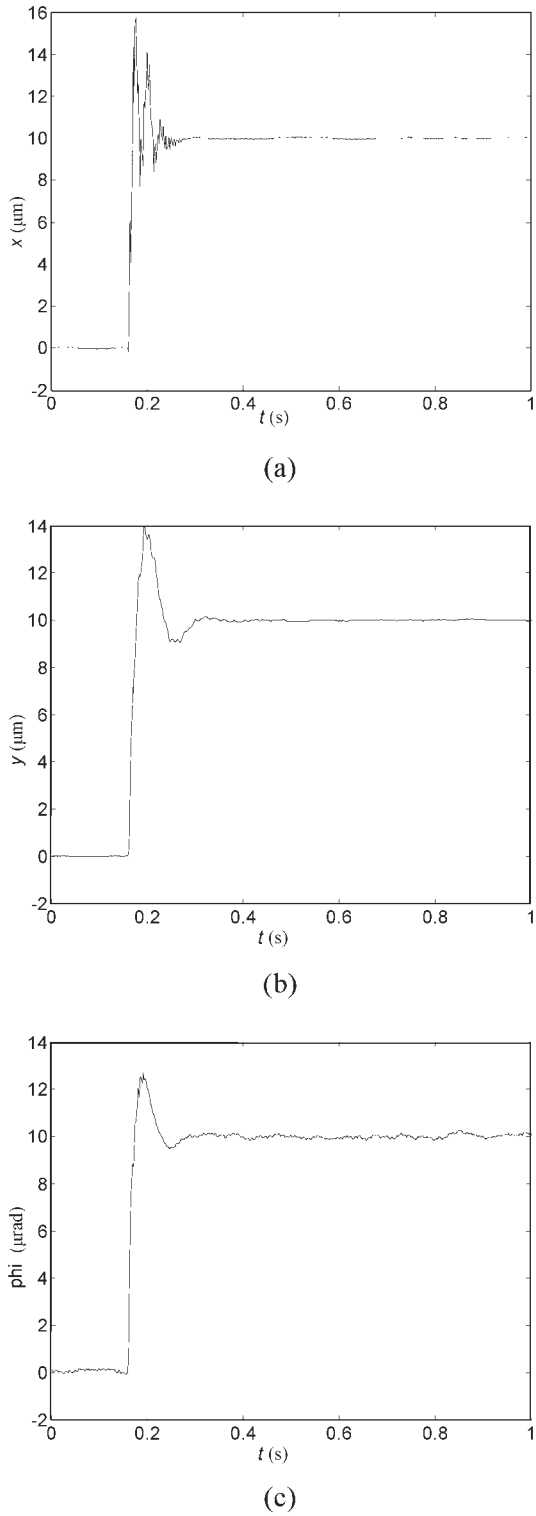

Fig. 7 (a), (b) 10 μm step responses in (a) x and (b) y; (c) 10 μrad step response in ϕ

of the ambient factors and the improvement in the absolute accuracy are beyond the scope of this research.

The multidimensional stage presented herein currently shows a maximum velocity of 0.4 m/s with 2 m/s^2 maximum acceleration. Thus it can traverse a range of

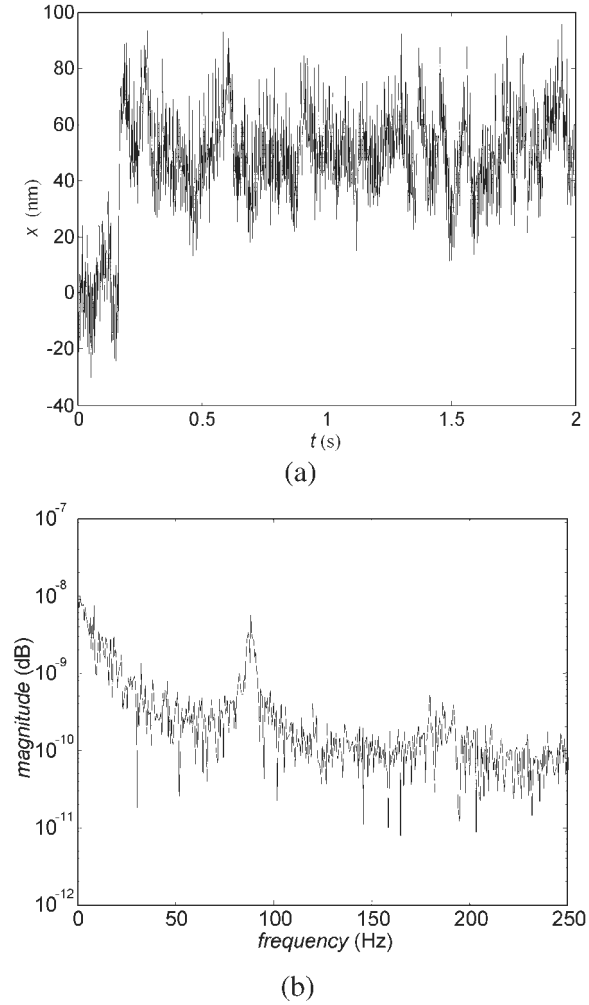

Fig. 8 (a) 50 nm step response in x; (b) frequency response of 50 nm step response in x

140 mm in just 550 ms. Figure 10a shows a 140 mm step response in the y direction. The initial and final acceleration of the stage is set at $\frac{1}{5}g$ (2 m/s^2) for 200 ms and the maximum velocity at 0.4 m/s. The stage reaches the

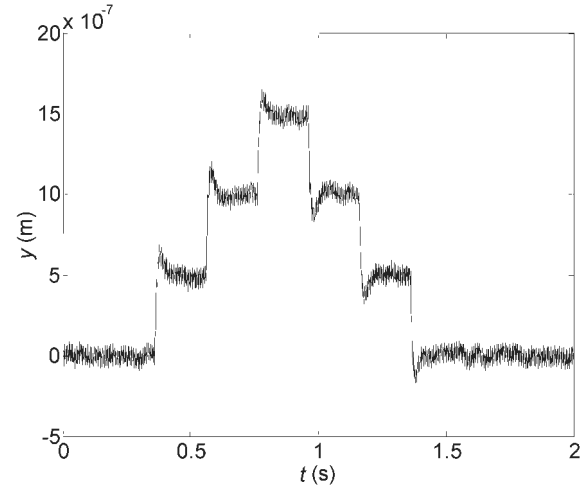

Fig. 9 500 nm staircase response in y

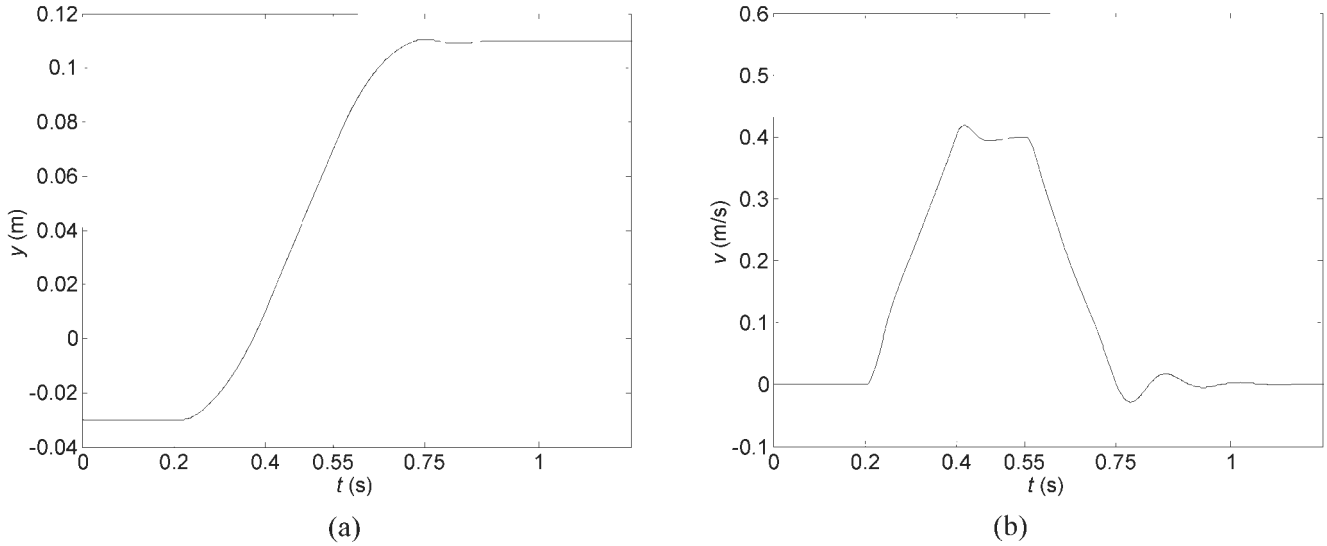

Fig. 10 (a) Position and (b) velocity profiles in y with 0.4 m/s maximum velocity and 2 m/s^2 maximum acceleration

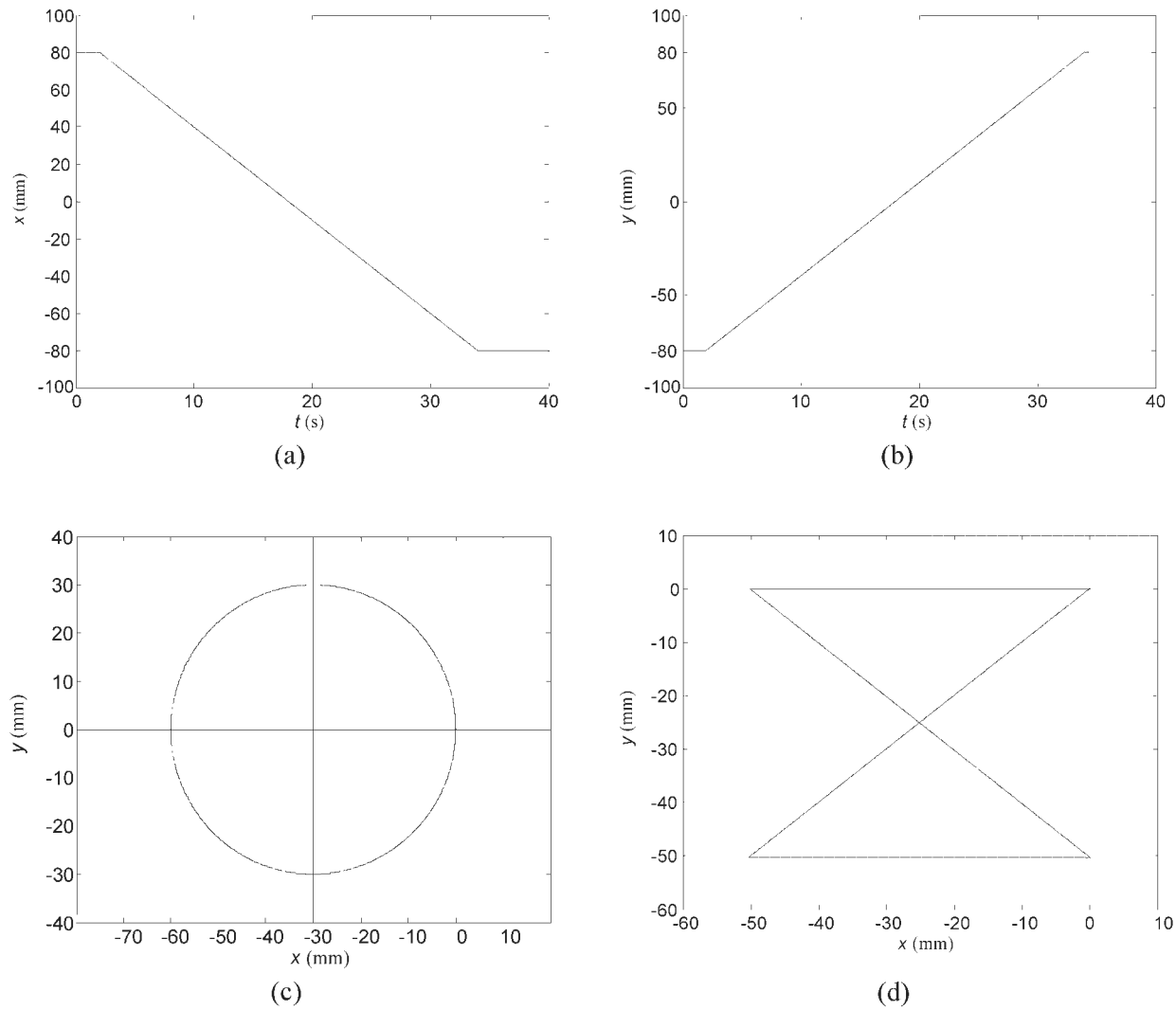

Fig. 11 (a), (b) 160 mm travel range traversed in both (a) x and (b) y; (c), (d) capability of following arbitrary planar paths in (c) a circle of 3 cm radius and (d) a double triangle

final positions in 550 ms as commanded. Figure 10b shows a corresponding trapezoidal velocity profile generated by the positioner.

This prototype stage has a travel range of 160 mm in both x and y. Figures 11a and b show that the platen moved 160 mm with a step increment of $\pm 2\,\mu$m per 0.4 ms in x and y respectively. Furthermore, this multi-dimensional positioner has the capability of following large arbitrary planar paths. Figures 11c and d show that the positioner followed a circular motion trajectory with a radius of 3 cm and a triangular motion trajectory.

7 CONCLUSIONS

In this paper, the design and construction of a novel integrated multidimensional positioner are presented. It has only a single-moving platen with a 5.91 kg mass and is based on a patented concentrated-field magnet matrix with dimensions of $304.8\,\text{mm} \times 304.8\,\text{mm} \times 12.7\,\text{mm}$. The moving platen carries multiphase windings, and the concentrated-field magnet matrix was assembled in the stationary base plate. Three aerostatic bearings were used to levitate the platen. The Pentek 4284 board with a TMS320C40 DSP was employed to perform real-time digital control of the system. Three interferometers provided three-DOF position information of the platen at a position resolution of 0.6 nm. Three laser distance sensors were utilized to monitor the air gaps between the aerostatic bearings and the base plate.

After implementing digital feedback controllers, a position resolution of 30 nm with a position noise of 10 nm r.m.s. in both x and y was achieved, as seen in the presented 50 nm step response. The position repeatability is 30 nm, and the platen dimensional stability is 32.7 μm. This prototype positioner has a planar travel range of $160\,\text{mm} \times 160\,\text{mm}$, which can be easily extended. It achieved a 0.4 m/s speed at an acceleration of $2\,\text{m/s}^2$ and could traverse 140 mm in just 550 ms. The large arbitrary planar motion generation capability of this positioning stage was demonstrated by producing motion profiles such as a circle of 3 cm radius and a double triangle.

This integrated positioner demonstrated an extended planar travel range and could follow both straight-line and curved paths in the xy plane with high position resolution. Thus this positioner can meet both the coarse- and the fine-motion requirements in semiconductor manufacturing. It is also highly suitable for many other applications in high-precision planar motion control such as scanners, computer numerical control machines and plotters. Thus this integrated positioning technology is a significant technological breakthrough in multi-dimensional positioning for precision manufacturing applications.

ACKNOWLEDGEMENTS

This material is in part based upon work supported by the Texas Advanced Technology Program under Grant 000512-0225-2001. The authors would like to thank Andy Ngai, Paul Fleener and Mike Mercer of Accurate Machine Works for their help in the assembly of magnet matrix and fabrication of the parts. Jie Gu, a former graduate student of Won-jong Kim, developed most of the user interface code.

REFERENCES

1 **Baskin, C. H.** Challenges in 300-mm wafer assembly. *Solid State Technol.*, July 1997, **40**(7), 131–140.
2 **Sawyer, B. A.** Magnetic positioning device. US Pat. 3,376,578, April 1968.
3 **Pelta, E. R.** Two-axis Sawyer motor for motion systems. *IEEE Control Systems Mag.*, October 1987, **7**(5), 20–24.
4 **Pelta, E. R.** Two axis Sawyer motor. In Proceedings of the 12th Annual IEEE Industrial Electronics Society Conference, Urbana, Illinois, 1986, pp. 3–8.
5 Normag *Northern Magnetics Linear Motor Technology Manual*, 1998 (Northern Magnetics, Inc., A Baldor Electric Company, Santa Clarita, California).
6 **Asakawa, T.** Two dimensional precise positioning devices for use in a semiconductor apparatus. US Pat. 4,535,278, August 1985.
7 **Ebihara, D.** and **Watada, M.** Study of a basic structure of surface actuator. *IEEE Trans. Magn.*, 1989, **25**(5), 3916–3918.
8 **Tomita, Y.** and **Koyanagawa, Y.** Study of a surface-motor driven precise positioning system. *J. Dynamic Systems, Measmt Control*, 1995, **117**, 311–319.
9 **Buckley, J. D., Galburt, D. N.** and **Karatzas, C.** Step-and-scan lithography using reduction optics. *J. Vac. Sci. Technol. B*, 1989, **7**(6), 1607–1612.
10 **Kim, W.-J.** and **Trumper, D. L.** Velocity regulation limits in a precision two-dimensional magnetic levitator. In Proceedings of the IEEE International Magnetics Conference, Kyongjoo, Korea, May 1999, paper EE-09.
11 **Kim, W.-J.** High-precision planar magnetic levitation. PhD thesis, Department of Electrical Engineering and Computer Science, Massachusetts Institute of Technology, Cambridge, Massachusetts, June 1997.
12 **Trumper, D. L., Kim, W.-J.** and **Williams, M. E.** Magnetic Arrays. US Pat. 5,631,618, May 1997.
13 **Halbach, K.** Design of permanent multipole magnets with oriented rare earth cobalt material. *Nucl. Instrum. Meth.*, 1980, **169**(1), 1–10.
14 **Kim, W.-J., Trumper, D. L.** and **Lang, J. H.** Modeling and vector control of planar magnetic levitator. *IEEE Trans. Industry Applic.*, 1998, **34**(6), 1254–1262.
15 **Oberg, E., Jones, F. D., Horton, H. L.** and **Ryefel, H. H.** *Machinery's Handbook*, 24th edition, 1992, p. 356 (Industrial Press, New York).